GEOPHYSICS, VOL. 47, NO. 7 (JULY 1982); P. 1068–1077, 13 FIGS.

Transient fields of a current loop source above a layered earth

G. M. Hoversten* and H. F. Morrison*

ABSTRACT

The electric field induced within four layered models by a repetitive current wave form in a circular loop transmitter is presented along with the resulting magnetic fields observed on the surface. The behavior of the induced electric field as a function of time explains the observed sign reversal of the vertical magnetic field on the surface. In addition, the differences between magnetic field responses for different models are explained by the behavior of the induced electric fields. The pattern of the induced electric field is shown to be that of a single "smoke ring," as described by Nabighian (1979), which is distorted by layering but which remains a single ring system rather than forming separate smoke rings in each layer.

INTRODUCTION

Quantitative interpretation of electromagnetic (EM) prospecting systems has led to elegant mathematical algorithms for computing the fields over layered and inhomogeneous earth models from a variety of transmitters. Often these solutions make it difficult to understand the basic EM phenomena that are occurring; this in turn makes the initial interpretation by the geophysicist rather abstract or mechanical. Continuing discussions of the relative merits of time-domain and frequency-domain systems are often based on limiting or asymptotic forms for the solutions. Rarely have the solutions been analyzed in terms of the basic physics of the governing Maxwell's equations. Recently, a thorough study of electric fields in a two-layer half-space in the frequency domain was presented by Pridmore (1978); studies of the transient electric fields in a half-space were presented by Lewis and Lee (1978) and Nabighian (1979). These studies have been very useful in explaining the fields observed on the surface in terms of the currents induced in the half-space.

As part of a larger study of time-domain and frequency-domain EM systems, we have developed algorithms for calculating time-domain electric fields in layered half-spaces. The solutions are first obtained in the frequency domain with methods described by Morrison et al (1969), then transformed to the time domain for a variety of source waveforms. The solutions are completely general, including displacement currents, and for the horizontal loop source they include a variable loop radius.

Apart from the general interest of finding a sound physical interpretation of fields measured on the surface over layered models, we have found the solutions for the electric (**E**) field in the ground very helpful in understanding the response of inhomogeneities in a layered half-space.

PARAMETERS OF THE SOLUTIONS

The particular results discussed here are taken from a larger study of a field system. Thus the choice of waveform, transmitter loop size, etc. has not been completely arbitrary. The results obtained are for the transmitter waveform shown in Figure 2. The repetition period is 1 sec and the transmitter loop radius is 56.4 m, yielding a loop area of 10^4 m^2. All calculations are for a unit dipole moment. The solutions have been checked in the frequency domain by comparison with models presented by Pridmore (1978) and in the time-domain by comparison with Nabighian (1979) and Morrison et al (1969). Although Nabighian used a rectangular loop, the results for a circular loop of equal area agree with Nabighian to better than 1 percent for a ratio of time divided by conductivity greater than or equal to 0.1.

The frequency-domain calculation of **E** within the layers was done by numerical integration which limited how near the loop solutions could be calculated accurately because of problems with

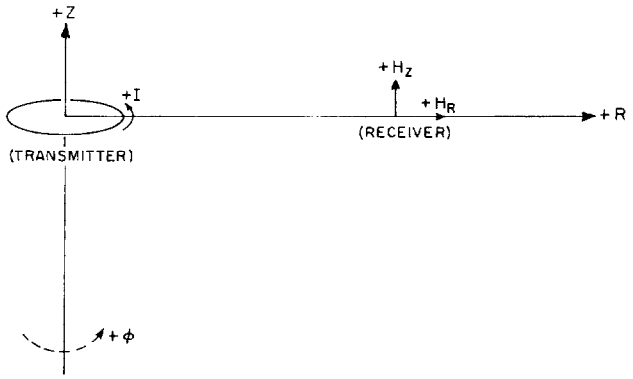

FIG. 1. Transmitter-receiver geometry.

Manuscript received by the Editor September 23, 1980; revised manuscript received April 27, 1981.
*Earth Sciences Division, Lawrence Berkeley Laboratory, University of California, Berkeley, CA 94720.

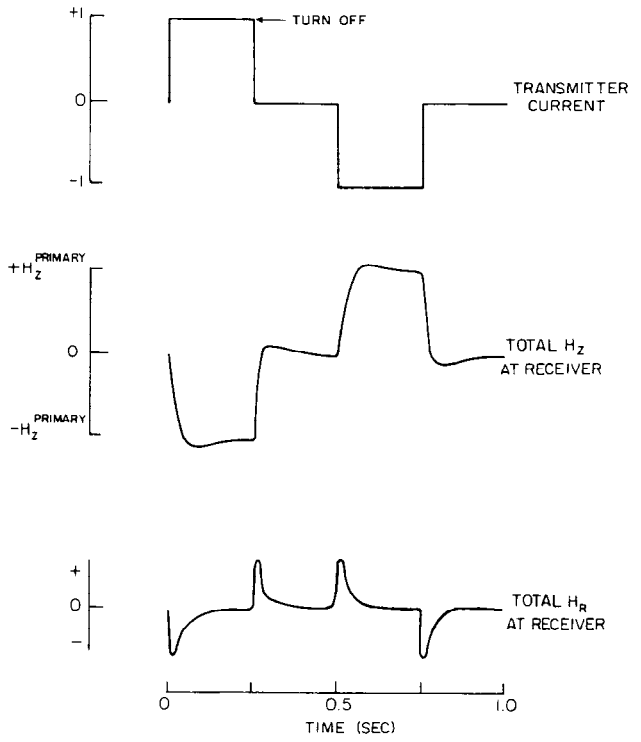

FIG. 2. Transmitter waveform and expected receiver signals.

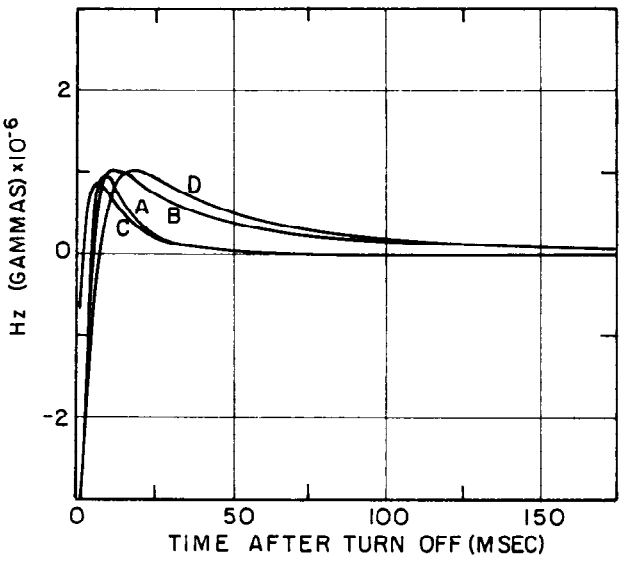

FIG. 4. Vertical **H** field at $R = 300$ m, linear scale.

convergence of the Hankel transform integral. Solutions nearer the loop could be obtained at greater expense; however, this was deemed unnecessary for an understanding of the cause-and-effect relationship between induced **E** and the observed magnetic fields on the surface for practical application. Thus all electric fields (in volts/meter) are presented on a cross-section with $R_{min} = 200$ m and $R_{max} = 450$ m, where R is the distance from the loop center. The depth extent of the cross-section is 250 m below the surface, and the sampling interval is 10 m in both directions.

A few words are needed to clarify the sign conventions. The coordinate geometry is shown in Figure 1, the z-coordinate axis is positive upward, and the positive ϕ direction is taken counterclockwise. The moment of the loop shown in Figure 1 with $+I$ current is also positive. At any radial distance from the center of the loop, the primary H_z field is negative or 180 degrees out of phase with the current in the loop.

Figure 2 shows the general behavior of (a) transmitter current, (b) total H_z at the receiver, and (c) total H_R at the receiver over a half-space. All magnetic and electric fields are shown after the downgoing edge of the positive section of the transmitter current, marked "turn off" in Figure 2. The induced **E** from the dB/dt of the falling current in the transmitter is in the positive ϕ direction, causing secondary currents to flow in the $+\phi$ direction. Figure 2

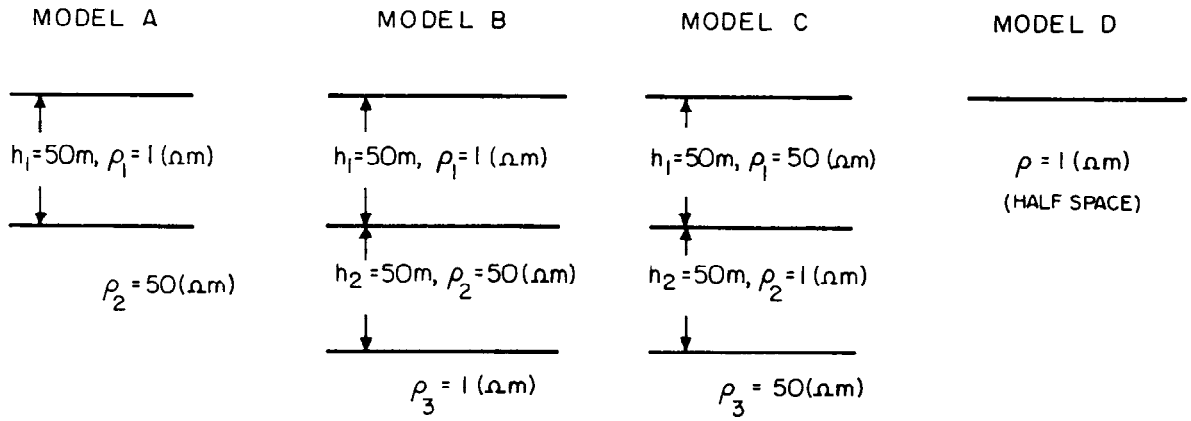

FIG. 3. The four models examined.

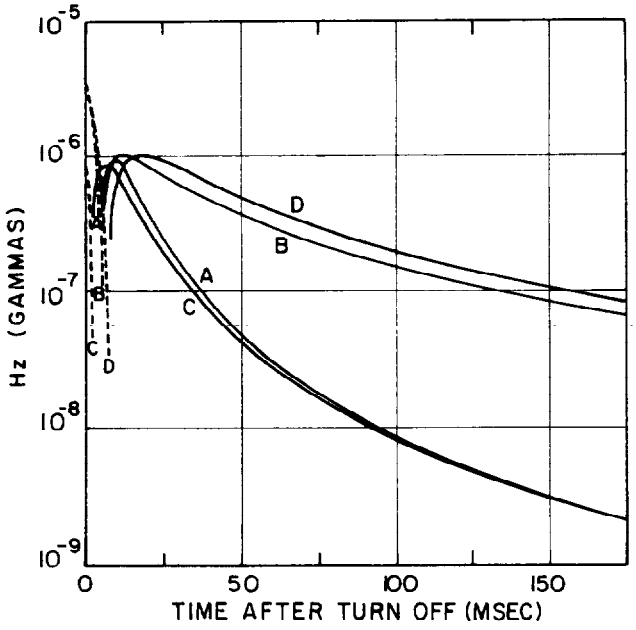

FIG. 5. Vertical **H** field at $R = 300$ m, $\log_{10}$ scale.

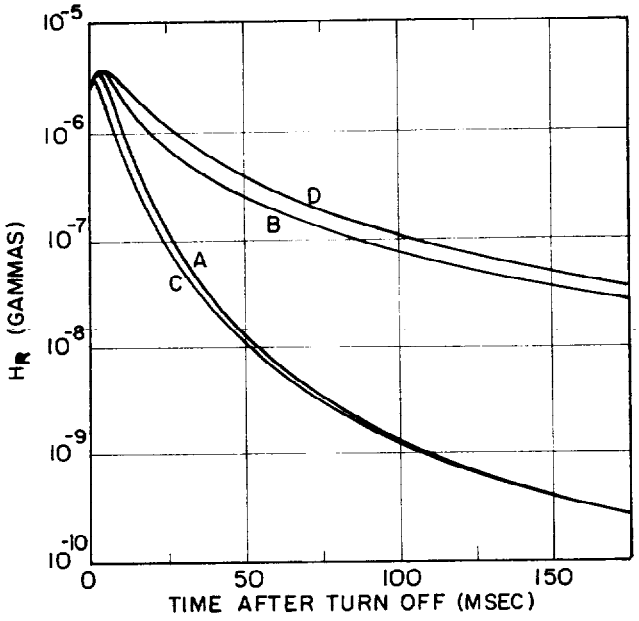

FIG. 7. Radial **H** field at $R = 300$ m, $\log_{10}$ scale.

represents the field behavior in general, giving the correct shape and sign in each section of the transmitted waveform; explanations of the details of this response will be given in the discussion that follows.

The four models chosen to illustrate the behavior of the fields are shown in Figure 3. We have chosen to analyze the relationship between surface magnetic fields at $R = 300$ m and subsurface electric fields (currents). The vertical magnetic field is shown in Figure 4 on a linear scale and in Figure 5 on a $\log_{10}$ scale. The radial magnetic fields are shown in Figure 6 on a linear scale and in Figure 7 on a $\log_{10}$ scale. The total **H** is shown in Figure 8 with a few times (in msec) after turn off.

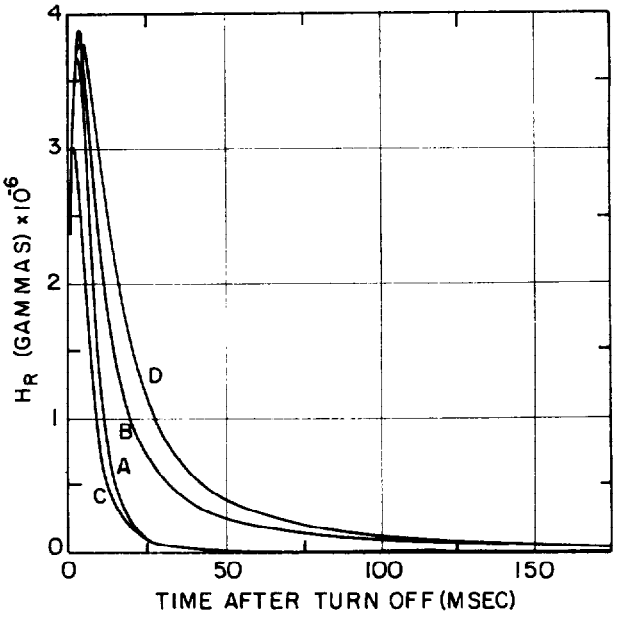

FIG. 6. Radial **H** field at $R = 300$ m, linear scale.

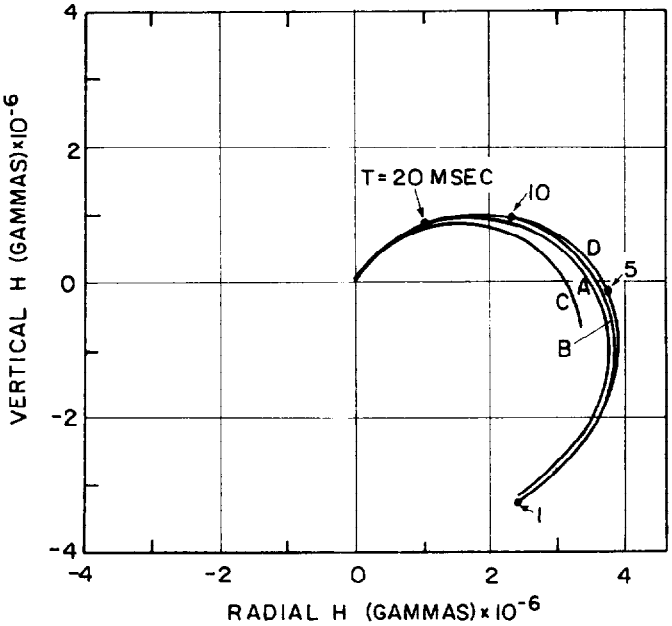

FIG. 8. Total **H** at $R = 300$ m, linear scale.

COMMON CHARACTERISTICS OF THE RESPONSES

Transient responses over layered models have common characteristics which reflect the common propagation characteristics of the induced **E** field within all layered models. The dominant feature of the propagation of induced **E** within the layered models is the concentric pattern of amplitude contours centered about a single maximum $\mathbf{E}_{max}$, which propagates away from the transmitting loop. Figure 9 shows this behavior for a 1 Ω-m halfspace (model D). The system of actual induced electric fields (currents) in a conductive earth resembles a system of smoke rings blown by the transmitter loop. As Nabighian (1979) pointed out, the magnetic field generated by these currents can be approximated by the field of a single fictitious current filament

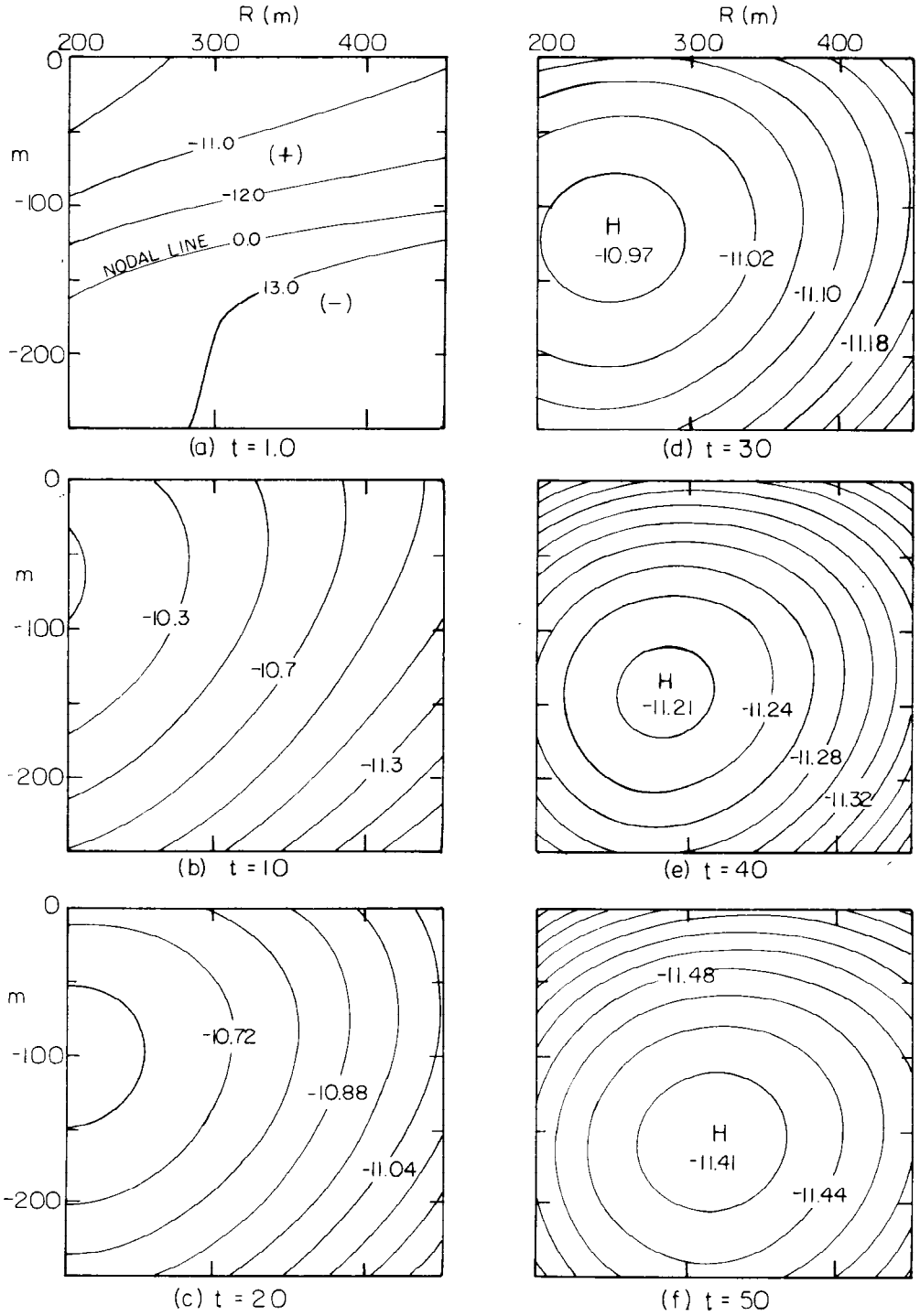

FIG. 9. Induced **E** (volts/m) field within model D.

which moves downward and outward with decreasing amplitude. The fictitious current element moves away from the loop at a greater angle (47 degrees) to the surface and at greater velocity than does $\mathbf{E}_{max}$ of the actual current system. At any time after turn off of the square wave, the fictitious current filament will be farther from the transmitter center and deeper than $\mathbf{E}_{max}$.

When relating the H_z zero-crossing time to the position of the fictitious single current filament or $\mathbf{E}_{max}$, one must remember the contribution of the currents on the opposite side of the transmitter. These currents produce magnetic fields which oppose the magnetic fields from ground currents within the cross-section we are considering. The result is that the H_z zero crossing will occur before either the single current filament or $\mathbf{E}_{max}$ reaches a position beneath the receiver. Although the fictitious single current and $\mathbf{E}_{max}$ propagate along different paths, they do so in the same general direction. The velocity of their propagation is similarly affected by changes in conductivity encountered as they move away from the transmitter, i.e., they both speed up in resistive ground and slow down in conductive ground.

Consider an area bounded on top by the earth's surface, on the

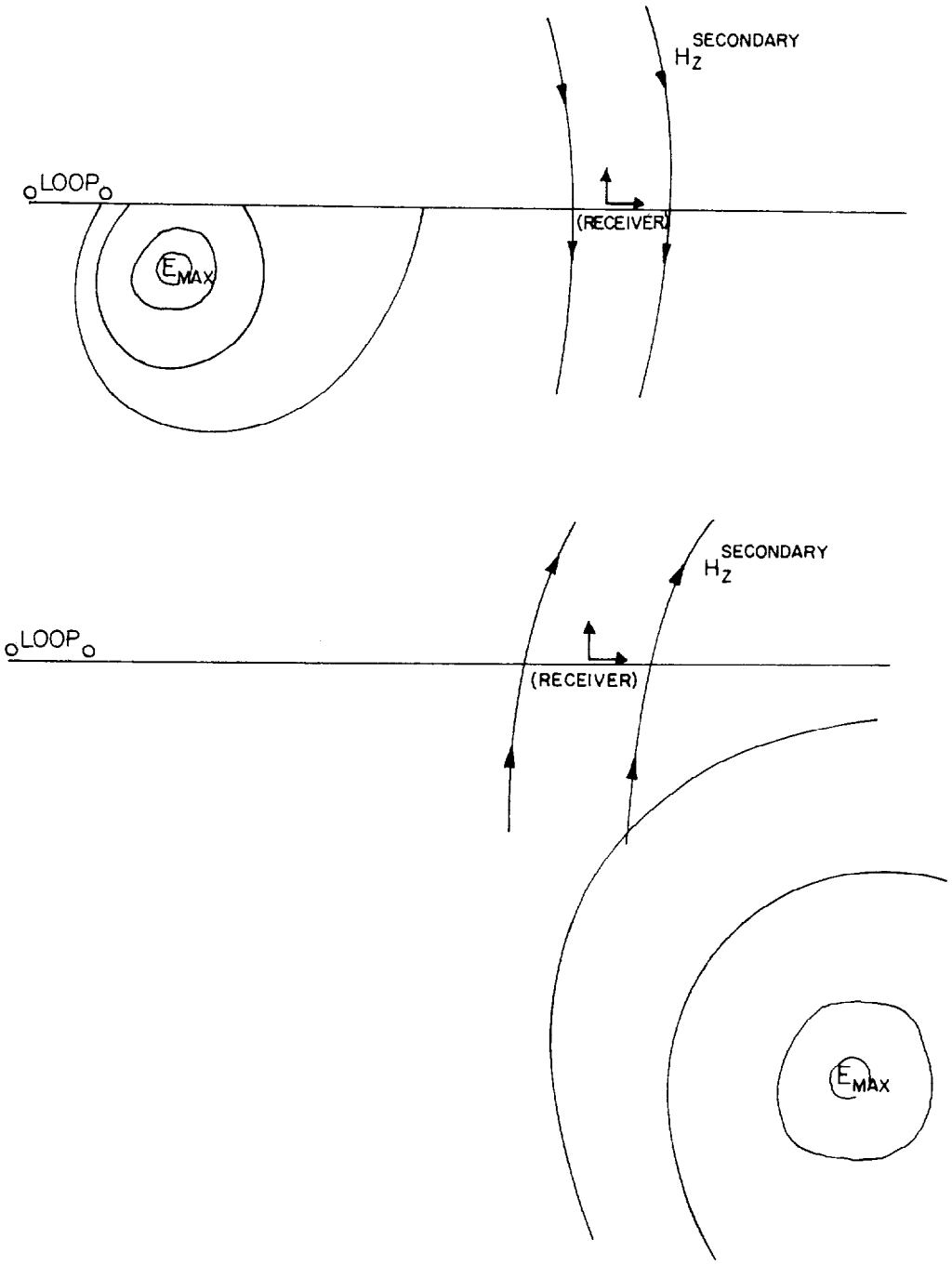

FIG. 10. (a) Relationship between E field and secondary H_z at early times. (b) Relationship between E field and secondary H_z at late times.

left by the transmitter center, and on the right and bottom by the position the fictitious single current filament has reached when H_z equals zero. Denote this area as the AVA. The H_z zero-crossing time is equal to the horizontal dimension of this area divided by the average horizontal velocity of the single current filament within this area. Although we have not computed the equivalent single current filament for these layered models, the concept of the average horizontal velocity of the current filament or of the actual $\mathbf{E}_{max}$ is useful in understanding the relationship of the zero crossings and peaks of the magnetic field responses to the layered structure which produced them. If one takes a square cross-sectional area of the models defined by the source-receiver separation as an approximation to the AVA, the order (from high to low) of the average horizontal velocity of $\mathbf{E}_{max}$ within the models corresponds to the order (from earliest to latest) of the H_z zero-crossing time.

HALF-SPACE RESPONSE

The induced electric field for the 1 Ω-m half-space (curve D) is shown in Figure 9 at times after turn off of 1, 10, 20, 30, 40, and 50 msec. This half-space response is the same as in Nabighian (1979) and Lewis and Lee (1978), with the exception of the **E** field shown at 1 msec. The latter authors used step function waveforms, whereas we have used a repetitive alternating waveform. Hence, at very early times after turn off, the earth at large distances is still responding to the pulse of opposite polarity, as shown in Figure 9a. The **E** below this nodal zone has a negative polarity caused by the rise of the square wave, while **E** above the nodal zone has a positive polarity caused by the fall of the square wave. The contours are of $\log_{10}$ of the amplitude with the sign added after taking $\log_{10}$. For example, in Figure 9a the -12.0 contour represents an **E** field equal to $+10^{-12.0}$ and the $+11.0$ contour represents an **E** field of $-10^{-11.0}$. It is worth noting that in conductive ground at large distances this combination of **E** polarities can result in a negative radial field at early times.

The electric field contours form a concentric pattern with a central maximum $\mathbf{E}_{max}$. This pattern, the moving smoke ring of **E** as Nabighian calls it, accounts for the sign reversal at H_z, as shown in Figure 10. For reasons noted above, the zero crossing of the H_z decay is earlier than the time when $\mathbf{E}_{max}$ passes directly below the receiver position. As noted by Lewis and Lee (1978) and Nabighian (1979), the position of $\mathbf{E}_{max}$ at late times moves off from the transmitter loop at ≃30 degrees, 28 degrees in this example.

CONDUCTIVE SURFACE LAYER (MODEL A)

Figure 11 shows the induced **E** field for a two-layer case where $\rho_1 = 1\ \Omega$-m, $h_1 = 50$ m, and $\rho_2 = 50\ \Omega$-m (curve A). Figure 11a shows that the nodal zone has already propagated beyond our cross-sectional area because of the increased resistivity of the lower half-space.

The fundamental difference between this model and the 1 Ω-m half-space is that $\mathbf{E}_{max}$ is confined to the surface conductor and does not penetrate the lower resistor within the time interval shown. The propagation velocity of $\mathbf{E}_{max}$ is proportional to the conductivity of the medium and inversely proportional to the time, so the velocity of $\mathbf{E}_{max}$ decreases with time. This explains the apparent difference in velocities of $\mathbf{E}_{max}$ in Figures 9 and 11 since the times at which $\mathbf{E}_{max}$ is within the cross-section are earlier for model A than for model D. At identical times after turn off, $\mathbf{E}_{max}$ propagates at identical velocities in media of identical conductivity with the direction of propagation affected by spatial changes in conductivity.

At early times, as shown by Figures 4 and 6, the vertical and radial magnetic fields for models A and D are identical. This corresponds to the times when the smoke ring of **E** in the thin top conductor is identical to the half-space **E** pattern. However, at times greater then 10 msec after turn off, the vertical and radial **H** response for model A falls below the half-space response. This is caused by a combination of factors: (1) The total current in the half-space is greater than that of the thin surface conductor, and (2) $\mathbf{E}_{max}$ for model A propagates horizontally, while $\mathbf{E}_{max}$ for model D propagates downward and outward yielding a horizontal component of velocity for model A which is greater than the horizontal component of velocity for model D. The increased horizontal velocity of $\mathbf{E}_{max}$ in model A compared to model D yields (1) an earlier H_z zero crossing for model A compared with model D, and (2) a reduced H_z for model A compared with model D, since at a given time $\mathbf{E}_{max}$ is horizontally farther from the receiver in model A then in model D. Radial **H** for model A is less than that for model D at late times because $\mathbf{E}_{max}$ is trapped near the surface in model A, where it is in a geometrically unfavorable position for producing H_R at the receiver, compared with the position of $\mathbf{E}_{max}$ in model D.

One other point is worth noting for model A: Figure 11a appears to indicate that a secondary maximum of **E** is propagating in the lower layer and because of a lower conductance moves through our cross-section between the frames shown. However, we examined the cross-section at times between those shown in Figures 11a and 11b, and there is no lower layer secondary maximum. There is only the one smoke ring which propagates in the conductor.

THREE-LAYER MODEL WITH MIDDLE CONDUCTOR (MODEL C)

The electric field within the three-layer model with $\rho_1 = 50\ \Omega$-m, $\rho_2 = 1\ \Omega$-m, $\rho_3 = 50\ \Omega$-m, and $h_1 = h_2 = 50$ m is given in Figure 12. The smoke ring pattern is very similar to that of model A. The $\mathbf{E}_{max}$ is confined again to the conductive layer. $\mathbf{E}_{max}$ has a higher propagation velocity within the surface resistive layer of model C than in the 1 Ω-m material at the surface of models A and D. This results in an initial increased horizontal displacement of $\mathbf{E}_{max}$ for model C as compared with models A and D. Once $\mathbf{E}_{max}$ has reached the middle conductive layer, its velocity is the same as that of $\mathbf{E}_{max}$ in models A or D. Comparison of Figures 11b and 12b shows that at 10 msec after turn off, $\mathbf{E}_{max}$ for model C is lower in amplitude and farther to the right than $\mathbf{E}_{max}$ for model A. The combination of surface high-velocity layer and the middle conductor, which confines $\mathbf{E}_{max}$ propagation within it to the horizontal direction, gives model C the highest average horizontal velocity between source and receiver and thus the earliest H_z crossing time.

After having peaked, the H_z and H_R responses for model C are less than those for model A because of the increased distance from the receiver position to the conductive layer and the increased ohmic losses incurred in model C as $\mathbf{E}_{max}$ propagates through the resistive surface layer. At late times the responses of A and C approach the same value of vertical **H** asymptotically. However, for radial **H** the decay curves cross at very late times and the response for model C becomes greater than the response for model A. This behavior is easily explained by considering the response at $R = 300$ m caused by a current filament which replaces the smoke ring of $\sigma \cdot \mathbf{E}_{max}$. At times $10 < t < 100$ msec after turn off, the equivalent filament for model A is below and nearer the receiver than the equivalent filament for model C; hence, there is a greater radial **H** for model A. However, at late times the equivalent filament for model A is still at the surface but far to the right. The angle $\angle_A$ between the filament and the

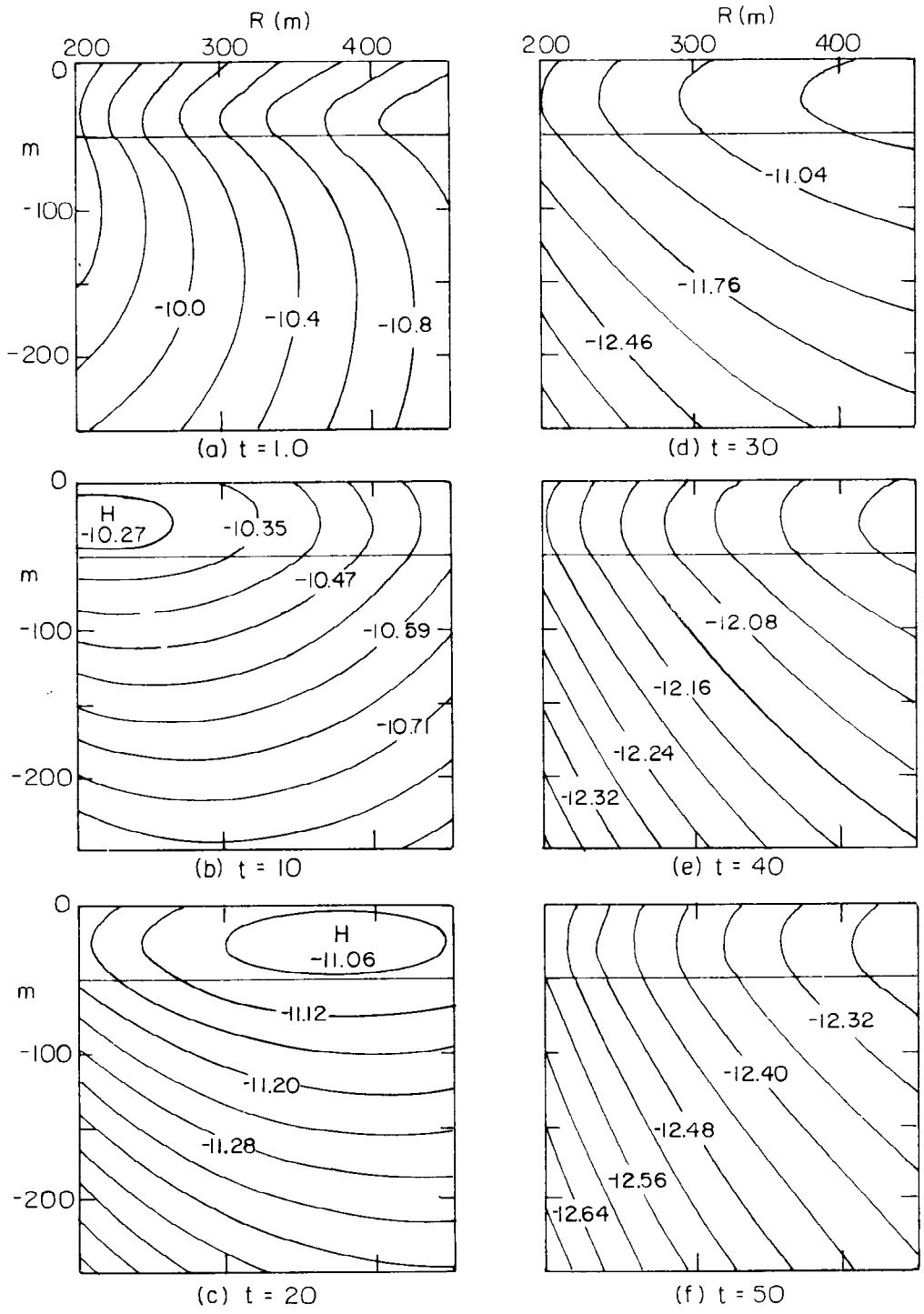

FIG. 11. Induced **E** field (volts/m) within model A.

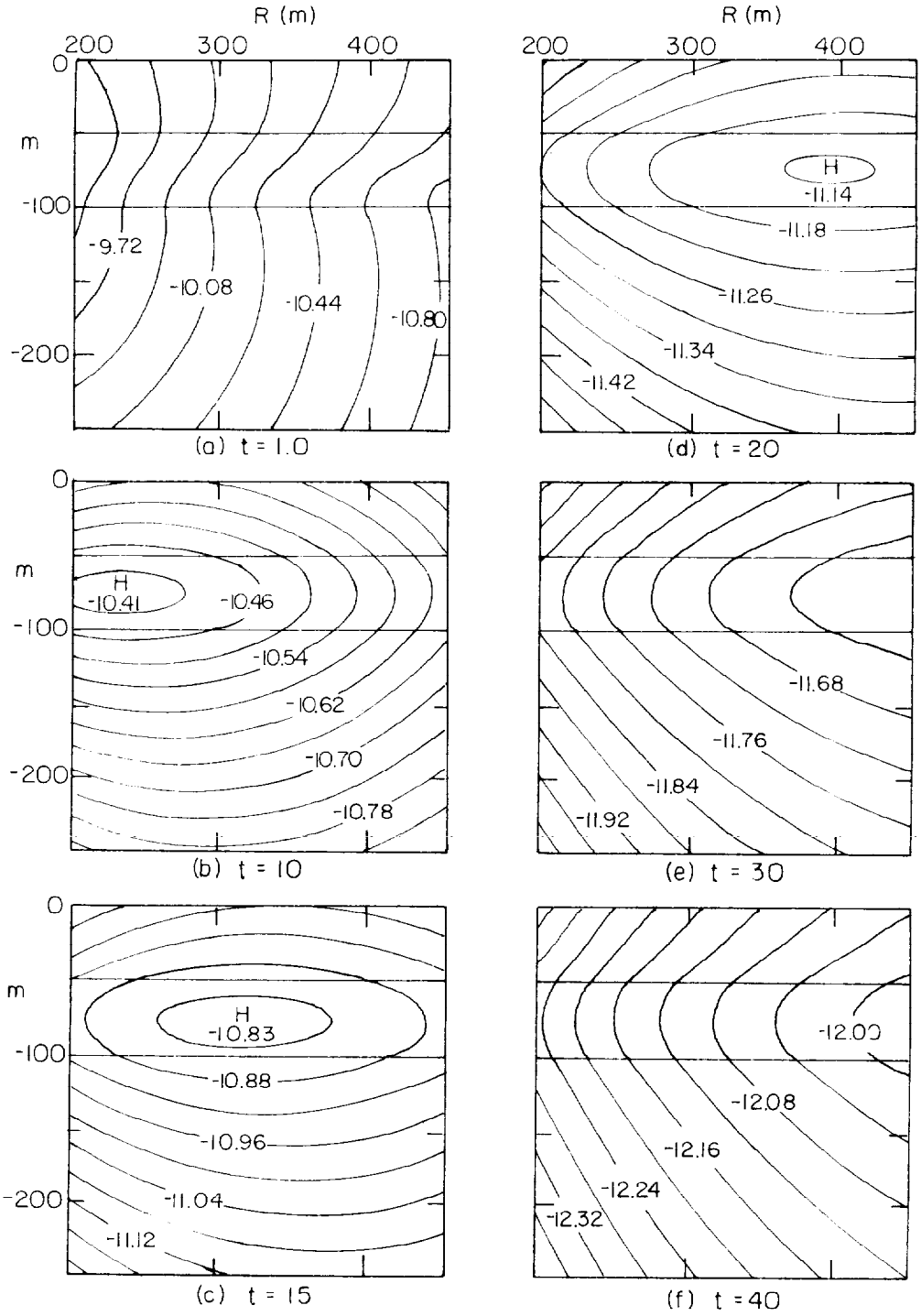

FIG. 12. Induced **E** field (volts/m) within model C.

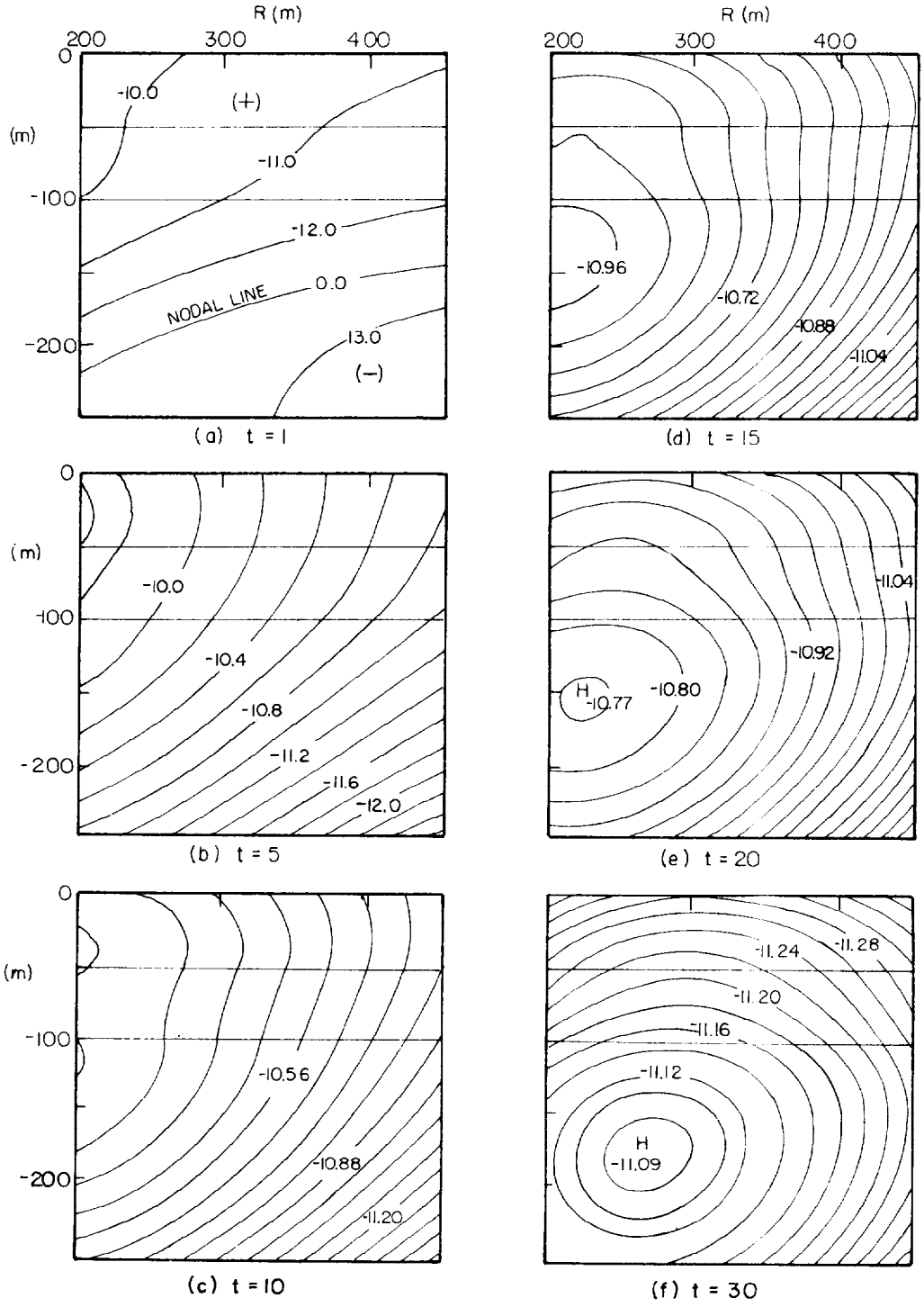

FIG. 13. Induced E field (volts/m) within model B.

horizontal plane of the receiver is ≈0 degrees, whereas the angle between the filament for model C and the horizontal plane of the receiver $\angle_C$ is greatert han $\angle_A$. It is this geometric relation which causes H_R for model C to be greater than H_R for model A at late times.

THREE-LAYER MODEL WITH RESISTIVE MIDDLE LAYER (MODEL B)

Figure 13 presents the **E** field within the model with $\rho_1 = 1.0$, $\rho_2 = 50$, $\rho_3 = 1$ Ω-m, and $h_1 = h_2 = 50$ m. The field pattern here is very similar to the 1 Ω-m half-space (model D) pattern. At 1 msec after turn off, the nodal line has moved a little farther out from the transmitter than for model D because of the resistive middle layer. At 5 msec after turn off, the $\mathbf{E}_{max}$ is confined to the surface conductor, as indicated on the left of Figure 13b. At 10 msec after turn off, as Figure 13c shows, the $\mathbf{E}_{max}$ seems to be splitting between the upper and lower layers; by 15 msec after turn off (Figure 13d) the $\mathbf{E}_{max}$ has totally penetrated the lower layer. After 15 msec, the smoke ring pattern is essentially that for a half-space with slight perturbation because of the thin resistor. At 20 msec (Figures 9c and 13e) the $\mathbf{E}_{max}$ for model B is lower and farther from the transmitter than $\mathbf{E}_{max}$ for the half-space (model D). From this time onward, the relationship between the two models remains constant, as seen in Figures 5 and 7 by the constant offset in the **H** field responses.

The presence of the conductive basement below the middle resistor acts to "pull" $\mathbf{E}_{max}$ out of the surface conductor through the middle resistor into the basement as time progresses. This keeps $\mathbf{E}_{max}$ from propagating entirely horizontally within the thin conductor as it does in models A and C and results in a reduced average horizontal velocity for model B compared with models A and C. The thin middle resistor does increase the average horizontal velocity for model C compared to the half-space model D. Thus, the H_z zero-crossing times as well as the H_z and H_R peak-value times for model C are greater than their corresponding times for models A and B and less than the corresponding time for model D.

CONCLUSIONS

By considering the induced **E** field within the earth, the behavior of the observed **H** fields on the surface for different models can be explained. In particular, the switch in polarity of the vertical **H** is easily visualized by considering a current filament which moves from the left of the receiver to the right of the receiver as time progresses. The crossover of radial field response for models C and A at late times is explained by a current filament trapped near the surface as opposed to a current filament trapped some distance below the surface.

In addition, it has been shown that rather than a system of smoke rings moving in each layer as might be expected, there is but one smoke ring which moves through the layering, which is distorted from the half-space pattern by the different velocities and attenuation rates of each layer.

ACKNOWLEDGMENTS

This work was performed for the U. S. Dept. of Energy, division of geothermal energy, under contract W-7405-ENG-48. We would like to thank Cary Hillebrand for working through the algebra to extend the solution for **E** field from the surface to within the layering.

REFERENCES

Lewis, R., and Lee, T., 1978, The transient electric fields about a loop on a half-space: Bull. Aust. SEG, v. 9, p. 173–177.

Morrison, H. F., Phillips, R. S., and O'Brien, D. P., 1969, Quantitative interpretation of transient electromagnetic fields over a layered half-space: Geophys. Prosp., v. 17, p. 82–101.

Nabighian, M. N., 1979, Quasi-static transient response of a conductive half-space—An approximate representation: Geophysics, v. 44, p. 1700–1705.

Pridmore, D. F., 1978, Three-dimensional modeling of electric and electromagnetic data using the finite element method: Ph.D. dissertation, Univ. of Utah.